Metallography, Microstructure, and Analysis (2023) 12:289–305
https://doi.org/10.1007/s13632-023-00935-5

PEER-REVIEWED PAPER

Early Efforts to Smelt Iron in Central Anatolia: Analysis of Iron Artefacts from the Bronze Age in Kaman-Kalehöyük

N. Kucukarslan[1] · T. Ota[1] · K. Kobayashi[1] · E. Nakamura[1] · S. Omura[2]

Received: 30 September 2022 / Revised: 13 December 2022 / Accepted: 1 January 2023 / Published online: 6 March 2023
© The Author(s) 2023

Abstract

A group of iron artefacts were excavated from the stratigraphic layers at Kaman-Kalehöyük in Central Anatolia, which were dated to the Middle and Early Bronze Ages. Some of them were re-analysed to discuss the state of iron production during such early periods, in terms of intentional carburization. The artefacts were re-examined via a minimally invasive approach by using optical microscope, scanning electron microscopy and energy dispersive spectroscopy to determine their chemical composition and microstructure. It was observed that the artefacts are composed of iron and/or steel. However, it is difficult to assert that they were produced as steel intentionally, because of their varying C contents and the lack of correlation between C content and artefact type. Such a finding could highlight the range in early efforts to smelt iron, while ancient metal workers were trying to figure out how to control furnace conditions during the Bronze Age in Central Anatolia.

Keywords Archaeometallurgy · Microstructure · Carbon Steels

Introduction

Iron production mainly consists of three main steps [1, 2]: (1) Smelting iron ore to produce bloom, (2) primary smithing to consolidate the iron and remove some impurities by hammering the bloom into a bar, thus creating a semi-product, and (3) secondary smithing to give the final shape to the object through a series of annealing and forging steps. Since metallic iron is soft, making an alloy with carbon (iron with up to 2 wt.% C is called steel) is one way of making iron harder and sturdier, which is termed carburization and is commonly viewed as a more advanced technology than iron smelting and forging alone. Pearlite, which is a lamellar structure with alternating cementite (Fe_3C) and ferrite layers, forms as a result of the carburization process [3–6]. Therefore, the presence of the pearlite and/or cementite structures in an ancient object indicates that it may have been originally crafted with a steel composition.

However, according to previous studies [4, 7], a technical difference was suggested between unintentional and intentional steel manufacturing, termed: *primary* and *secondary carburization*, respectively. The authors point out that the random absorption of C into the bloom might occur during smelting if a very C-rich and reductive environment is formed in the furnace. The result is the formation of cementite and pearlite in an ancient object, but its formation is unintentional [4, 7]. On the other hand, when an iron object with its final shape is immersed into a hearth with C-rich environment for a considerable time, it increases the C content in the iron object and makes the iron object harder, especially inwards from the edge of the object [2, 4]. If this step is performed in addition to simple forging and heating, it might indicate that the steel composition is formed intentionally. Furthermore, Eliyahu-Behar and Yahalom-Mack [2] state that even the secondary carburization is not enough to make iron harder and preferable over other metals like

This invited article is part of a special topical issue of the journal *Metallography, Microstructure, and Analysis* on Archaeometallurgy. The issue was organized by Dr. Patricia Carrizo, National Technological University – Mendoza Regional, and Dr. Omid Oudbashi, Art University of Isfahan and The Metropolitan Museum of Art, on behalf of the ASM International Archaeometallurgy Committee.

✉ N. Kucukarslan
pb0c6mjp@s.okayama-u.ac.jp

[1] Pheasant Memorial Laboratory for Geochemistry and Cosmochemistry, Institute for Planetary Materials, Okayama University, Yamada 827, Misasa, Tottori 682-0193, Japan

[2] Japanese Institute of Anatolian Archaeology of the Middle Eastern Culture Centre in Japan, Çağırkan, Kaman, Kırşehir 40350, Turkey

bronze. A series of heat treatments like quenching and tempering should be also undertaken to make iron harder and preferable in comparison with bronze, which was the most processed metal during the Bronze Age [2]. This complete *chaine operatoire* also demonstrates a more advanced technology than simple iron production. Iron objects produced by such an advanced technology started to be seen in significant numbers from the Iron Age onwards in Central Anatolia [8, 9] and evidence for their production prior to the Iron Age is not quite definitive.

However, based on cuneiform tablets from the Bronze Age, it is believed that the Hittites were skilled in ironmaking (ca. 1700–1200 BCE). In the Hittite texts, iron appears as a scarce source of valuable metal, which is used mostly as offerings in temples and gifts for the kings [10, 11]. When tracing back earlier, iron is one of the metals asserted in the ancient texts from the Assyrian Colony Period (**ACP**, ca. 2000–1700 BCE) [12] and iron is described as a very precious metal [13, 14]. Veenhof [15] also points out that iron was traded in small amounts, a couple of hundred grams at most. One story from the ancient texts [16] gave a clear picture of how lucrative the iron trade was during the ACP. Larsen [16] mentioned a *venture* in an ancient text from the archive of the Assyrian merchant *Salim-Assur*. The adventurous trade was to sell iron in the form of rings with the weight of 18¾ shekels of iron (ca. 156 g) for silver which was planned to pay the debt of 22½ minas of silver (ca. 11 kg). This corresponds to the exchange rate 73:1 [15, 16]. Why was iron so incredibly expensive? Dercksen [14] points out the inadequacy in ironmaking, which must have made iron so expensive when compared to other metals. The authors [14, 15, 17] also draw attention to the wide scale of prices for iron: from 11½ to 140 shekels of silver for 1 shekel of iron. Dercksen [14] considers '*the greatly varying degrees of purity*' as the reason behind this wide scale of prices. The difficulty in controlling the iron smelting process with a high reducing atmosphere and high temperature [18] might thus lead to the changes in quality of iron. However, this discussion based on textual sources poses the question: can such discussion be supported by archaeological evidence and were the iron materials in the archaeological record different enough in purity or quality to reflect on iron prices? Although which types of iron mentioned in the ancient texts are not distinguished clearly, it is commonly asserted that ore and iron bloom were mainly sold [14, 15]. Meanwhile, a group of iron artefacts were excavated from the stratigraphic layers of Kaman-Kalehöyük in central Anatolia, which were dated to the Middle Bronze Age (**MBA**, ca. 1930–1400 BC) and Early Bronze Age (**EBA**, the intermediate phase ca. 2100–1930 BC) (Fig. 1). Such artefacts may thus hold clues that can be used to answer the above question.

The above iron artefacts from the Bronze Age were studied in Akanuma [19–25]. Some of the artefacts were described in terms of their microstructure and composition. Subsequently, the steel composition with bright cementite lamella was recognized in the microstructural analysis. However, it was not thoroughly discussed if this steel composition was intentionally formed or not. Therefore, a group of iron artefacts from the MBA and EBA were re-examined in this study.

Also, another concern about such early iron artefacts is whether they were made from the iron extracted from terrestrial iron sources and thus smelted or were obtained from meteoric iron, which is composed of Ni–Fe alloy [26] and one of the main sources for iron during the Bronze Age [27–30]. The artefacts were thus re-analysed in terms of morphology, composition (dominant phases), concentration and distribution of C, in order to discuss their source (meteoric and terrestrial) and if intentional carburization was possible at such early periods.

Materials

Excavation and Stratigraphy

Kaman-Kalehöyük is an ancient mound in central Anatolia, about 100 km southeast of Ankara in Turkey. The ancient mound is 16 m in height and extends over a circular area 280 m in diameter [31] (Fig. 1). The excavation of the ancient mound is still ongoing, being undertaken by a team from the Japanese Institute of Anatolian Archaeology (JIAA) under the direction of Sachihiro Omura in 1985. There are three main excavations being conducted on the site: North Trench, South Trench and City-Wall Trench [31]. In the north trench, the excavation is being conducted on a smaller area but to greater depth to understand the overall stratigraphy of the ancient mound. The stratigraphy of Kaman-Kalehöyük has thus been established by the team throughout the excavations of the North trench, especially through tracing the main burnt stratigraphic layers between and within the main periods (Fig. 1). Accordingly, four main strata were determined in the ancient mound: Stratum I-Ottoman Empire and Byzantine Periods; Stratum II-Iron Age; Stratum III-Hittite Empire (IIIa), Old Hittite Period (IIIb) and Assyrian Colony Period (IIIc); Stratum IV-Intermediate Period (IVa) and Early Bronze Age (IVb). Radiocarbon analysis [32] was also performed on the charred wood and burnt wheat grains, which were collected from the stratigraphic layers with burnt architectural remains or burnt soil context, from Stratum IVb (EBA) to Stratum IId (Early Iron Age). Radiocarbon dating supplies the 1σ ranges of *2130–2105 and 2055–2030 cal. BC* for the boundary between the Stratum IVb (Early Bronze Age) and the Stratum IVa (Intermediate Period); and 1σ ranges of *2045–2010 and 2030–1890 cal. BC* for the boundary between the Stratum IVa (Intermediate

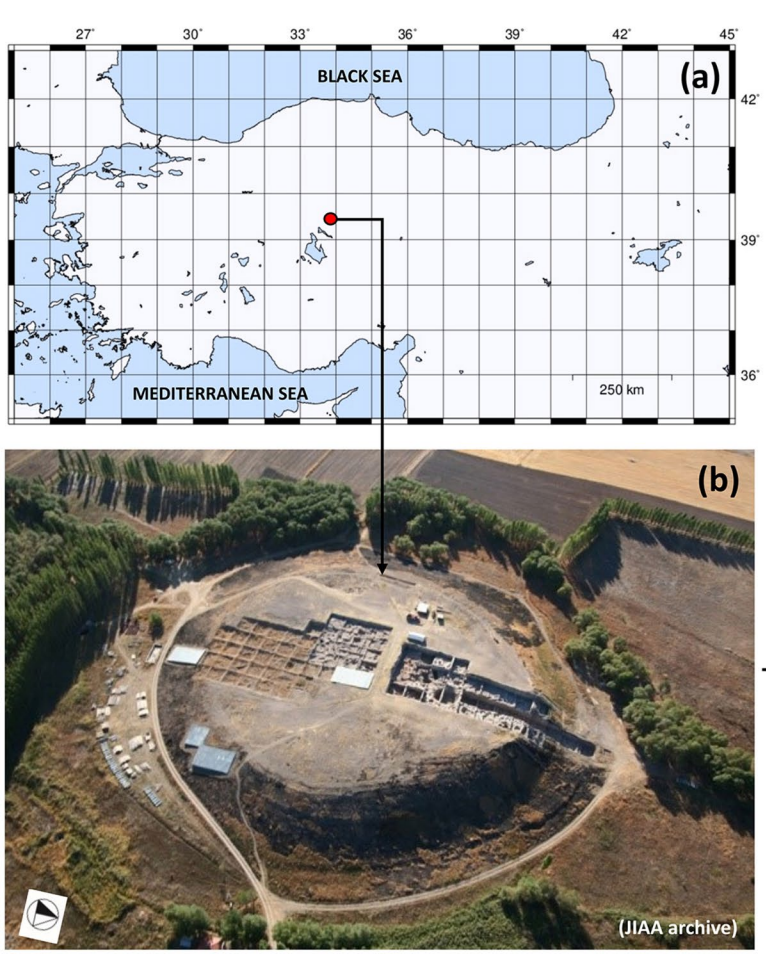

Kaman-Kalehöyük (c)

Date	Stratum		Period
ca. 1700 AD	I	a	Ottoman
ca. 1500 AD			
ca. 1400 AD		b	Byzantine
ca. 430 BC	II (Iron Age)	a	Hellenistic Late Iron Age
ca. 650 BC			
ca. 675 BC		b	Middle Iron Age (Phrygian Rule)
ca. 720 BC		c	Middle Iron Age (Alisar IV)
ca. 1200 BC		d	Early Iron Age
ca. 1400 BC	III (Late Bronze Age)	a	Hittite Empire
ca. 1700 BC	III (Middle Bronze Age)	b	Old Hittite
ca. 1750 BC		c	Assyrian Colony Period
ca. 1930 BC			
ca. 2100 BC	IV (Early Bronze Age)	a	Intermediate Period
ca. 2300 BC		b	Early Bronze Age
			Excavation Cont'd

Fig. 1 (**a**) Location, (**b**) aerial view, (**c**) stratigraphy and chronology of Kaman-Kalehöyük, the group of iron artefacts in this study were excavated from the stratigraphic layers highlighted in yellow

Period) and the Stratum IIIc (Assyrian Colony period) [32]. Radiocarbon dating supplies the 1σ ranges of *1765–1700 and 1745–1680 cal. BC* for the boundary between the Stratum IIIc (Assyrian Colony period) and the Stratum IIIb (Old Hittite period) [32]. Therefore, the MBA covers the Strata IIIb and IIIc; and the EBA covers the Strata IVa and IVb.

To find out the status of Kaman-Kalehöyük in the historical landscape, some of the distinguishing features of the ancient site during the MBA and EBA will be mentioned here. A group of enormous *Round Structures*, which are up to 10 m in diameter and up to 5 m in height, were uncovered from Stratum IIIb. In one of these structures, a great amount of fossilized remains of wheat was found [31]. This finding thus raised the possibility that these *Round Structures* might have been used as grain storages. If all of these enormous *Round Structures* were assumed to have been used as grain storage, the amount of wheat that could have been stored would be excessive, being much more than the local population would have required, considering the size of the site [31]. It thus strengthens the status of Kaman-Kalehöyük as a *regional distribution center* during the Old Hittite period [31]. From the Stratum IIIc, a nine-room complex which was completely burnt with a group of severely burnt skeletons including adults, children and infants was unearthed [31]. Many metallic items such as copper alloy daggers and spearheads were found together with the deceased burnt skeletons. When also considering the city wall, which was partly uncovered [33], the complex architectural remains and the finds made of gold such as an adornment for crown with a lion figure [34], Kaman-Kalehöyük might have had an important position during the MBA. During the EBA, the destroyed burnt context was also observed in the architectural remains from the Stratum IVa. The Stratum IVa is considered as a transitional period from the EBA to the ACP in the overall stratigraphy of the ancient

mound, because of the mixture of wheel-made and hand-made pottery in almost similar ratios [31].

Of the artefacts considered here, three were excavated from the Stratum IIIc of the MBA (Table 1), and two were from the stratigraphic layers between the Stratum IIIc and IIIb. These five artefacts are defined as the MBA artefacts in this paper. One iron artefact, which was excavated from the Stratum IVa of the EBA, is defined as the EBA artefact in this paper.

Morphology and Sample Conditions

The six iron artefacts, which are included in this study, were found as fragments with lengths of 1.5–4.2 cm. Although the artefacts are severely corroded and it is thus difficult to describe their morphology precisely, the EBA iron artefact K6 had a bar-like shape. From the MBA, two had a pin-like, one had pin- or nail-like shape, one had a knife-like, and one had a bar-like shape (Fig. 2).

Methodology

Sample Preparation

All sample preparation and analyses were conducted in the Pheasant Memorial Laboratory, Institute for Planetary Materials, Okayama University (Japan). The artefacts were re-examined in this study via a minimally invasive approach by analysing the surface that was exposed from cross-sectioning of the sample in the previous study. Only dry-polishing with a 3M™ Al_2O_3 lapping film was undertaken on the exposed sample surface, to remove a tiny layer of corrosion and the saw marks left from the previous study. Subsequently, the iron artefacts were analysed using an Olympus DSX-1000, optical microscope and a JEOL, JSM-7001F, field-emission scanning electron microscope (FE-SEM), without carbon-coating since they were conductive enough that severe electric charging did not occur. Furthermore, no chemical etching process was applied to the samples.

Analysis

To examine the microstructure and chemical composition, the artefacts were analysed using the FE-SEM, equipped with an Oxford, INCA X-act, energy dispersive spectrometer (EDS) with a silicon drift detector and Be window, and using the Oxford, AZtec software. The analyses of all the samples were conducted under operating conditions with an accelerating voltage of 15 kV, beam current of 5 nA and working distance of 10 mm. A series of spot analyses were conducted on the samples. The results of the spot analyses were calculated using the elements C, O, Na, Mg, Al, Si, P, S, Cl, K, Ca, Ti, Cr, Mn, Fe, Co, Ni, and Cu, and normalized to 100% in total. In this study, concentrations of Fe, O, and C were determined for the main phases like metallic iron, iron oxides in corrosion, iron carbide compounds. Nickel and Co were also analysed to evaluate whether or not the iron artefact was made from a material of a meteoric source. The results are displayed in weight percentages (wt.%) in Table 2. To evaluate the analytical results, standard error (wt.% sigma) is acquired from the EDS software. Each individual analysis has its own wt.% sigma deviation. Thus, there is a range of wt.% sigma values for each element,

Table 1 Excavation information concerning the iron artefacts in this study

Sample No	Morphology	Excavation Archive No	Trench	Sector	Provisional Layer No	Context	Chronology	Stratum	Period
K1	knife-shaped	06000691–1	North	VI	70	Artefact K2	Middle Bronze Age	IIIb–IIIc	Assyrian Colony Period—Old Hittite Period
K2	pin-shaped	06000691–2	North	VI	70	Artefact K1	Middle Bronze Age	IIIb–IIIc	Assyrian Colony Period—Old Hittite Period
K3	pin-shaped	07000281	North	VII	56	…	Middle Bronze Age	IIIc	Assyrian Colony Period
K4	nail- or pin-shaped	13000297	North	V	136	One slag piece	Middle Bronze Age	IIIc	Assyrian Colony Period
K5	bar-shaped	13000299–2	North	V	172	One slag piece	Middle Bronze Age	IIIc	Assyrian Colony Period
K6	bar-shaped	01000854	North	IV	73c	…	Early Bronze Age	IVa	Intermediate Period

Context indicates if there was any related architectural remain, e.g. a hearth or a material-like slag, which could be associated with iron smelting/smithing processes or another iron artefact from the same findspot

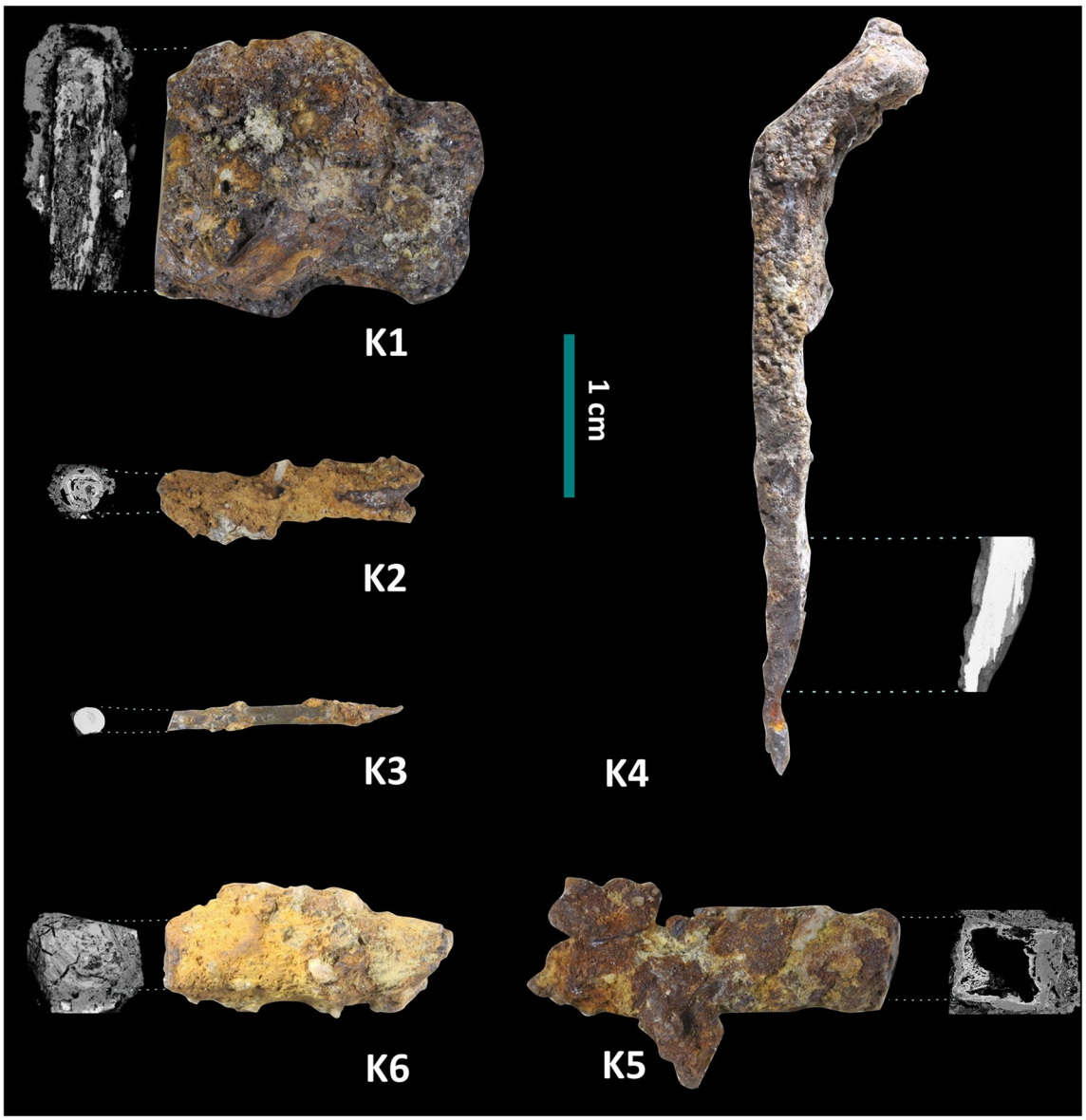

Fig. 2 Morphology of the iron artefacts. The photographs of the samples and their cross-sectional view in BSE mode under SEM–EDS. From the Middle Bronze Age (K1) knife-shaped iron artefact, (K2) pin-shaped iron artefact, (K3) pin-shaped iron artefact, (K4) pin- or nail-shaped iron artefact, (K5) bar-shaped iron artefact. From the Early Bronze Age (K6) bar-shaped iron artefact

which is obtained from the series of spot analyses (Table 2). If the element concentration is lower than wt.% sigma deviation, it is not included in the data set and shown as '–' in Table 2.

Estimation of C Content and Distribution

Although the sample surfaces contain corrosion pits [4], the surfaces were examined carefully in order to detect any area with pearlite remnants under SEM observation. Pearlite remnants could be detected in a lamellar pattern with relatively brighter or darker iron carbide layers [3] and were distinguished using the contrast enhancement and binary functions of the image processing software, NIH ImageJ 1.52a (Fig. 3). Subsequently, the relative percentage of the areas with pearlite remnants on the sample surface was calculated by the threshold function of the software (Fig. 3c). The percentage of pearlite remnants was multiplied by 0.8 which is the approximate weight percent of C in a pearlite compound [35]. A series of image analyses ($n = 4$–6 for each artefact, depending on the size and condition of the sample surface) were performed by applying the estimation method.

After all areas with pearlite remnants were examined, each analysed area is recorded with its location and C

Table 2 Average chemical compositions (wt.%) of the dominant phases in the iron artefacts

	wt.% Sigma (min–max)		C	O	Na	Mg	Al	Si	P	S
			0.3–0.9	0.1–0.8	0.07–0.20	0.04–0.13	0.04–0.11	0.03–0.09	0.04–0.1	0.03–0.09
Sample No.	**Phase**									
K1	Metallic iron									
	Bright-lamellar	avg ($n=3$)	9.6	11	–	–	–	–	–	–
		std	0.9	5	–	–	–	–	–	–
	Light grey	avg ($n=16$)	–	34.1	–	–	–	0.2	–	0.12
		std	–	0.9	–	–	–	0.1	–	0.05
	Grey	avg ($n=9$)	0.9	42.9	–	–	0.15	0.5	–	0.08
		std	0.1	0.4	–	–	0.07	0.2	–	0.01
K2	Metallic iron									
	Bright-lamellar	avg ($n=4$)	8	5	–	–	–	–	–	0.18
		std	2	1	–	–	–	–	–	0.01
	Light grey	avg ($n=9$)	–	34	–	–	–	0.3	–	0.16
		std	–	2	–	–	–	0.2	–	0.04
	Grey	avg ($n=7$)	–	42	–	–	0.14	0.3	0.11	0.3
		std	–	2	–	–	0.05	0.1	0.03	0.1
K3	Metallic iron	avg ($n=5$)	–	–	–	–	–	0.23	–	–
		std	–	–	–	–	–	0.04	–	–
	Bright-lamellar	avg ($n=9$)	5.5	0.8	–	–	0.17	0.25	–	–
		std	0.9	0.2	–	–	0.02	0.03	–	–
	Light grey									
	Grey	avg ($n=3$)	1.1	39.1	–	–	–	0.3	–	0.9
		std	0.2	0.6	–	–	–	0.1	–	0.1
K4	Metallic iron	avg ($n=24$)	1.3	–	–	–	0.18	–	0.3	–
		std	0.2	–	–	–	0.02	–	0.1	–
	Bright-lamellar	avg ($n=3$)	7.5	30.0	–	0.26	0.15	0.38	–	–
		std	0.8	2.1	–	0.03	0.01	0.03	–	–
	Light grey	avg ($n=8$)	–	34.3	–	–	–	0.12	0.2	0.18
		std	–	2.0	–	–	–	0.01	0.0	0.03
	Grey	avg ($n=34$)	3	39	–	0.4	0.3	0.7	0.2	0.25
		std	1	3	–	0.2	0.2	0.4	0.1	0.05
K5	Metallic iron	avg ($n=2$)	1.6	0.3	–	–	–	–	–	–
		std	0.8	0.1	–	–	–	–	–	–
	Bright-lamellar	$n=1$	8.4	12.0	–	–	–	–	–	–
	Light grey	avg ($n=28$)	–	32	–	0.11	–	0.2	0.10	0.16
		std	–	1	–	0.01	–	0.1	0.04	0.05
	Grey	avg ($n=22$)	0.8	43	0.18	0.3	–	0.8	0.2	0.11
		std	0.2	1	0.05	0.1	–	0.5	0.1	0.03
K6	Metallic iron	avg ($n=3$)	–	2.9	–	–	–	–	–	–
		std	–	0.5	–	–	–	–	–	–
	Bright-lamellar	avg ($n=11$)	4.8	25	–	–	–	0.2	–	0.16
		std	1.3	3	–	–	–	0.1	–	0.03
	Light grey	avg ($n=16$)	–	34.1	–	–	–	0.3	–	0.18
		std	–	0.9	–	–	–	0.1	–	0.07
	Grey	avg ($n=19$)	1.0	42	–	0.3	–	0.5	–	0.15
		std	0.2	1	–	0.2	–	0.4	–	0.04

Table 2 (continued)

			Cl	K	Ca	Ti	Cr	Mn	Fe	Co	Ni	Cu
	wt.%Sigma (min–max)		0.03–0.09	0.04–0.10	0.04–0.10	0.05–0.12	0.05–0.13	0.1–0.2	0.3–1.0	0.17–0.38	0.1–0.3	0.3–1.0
Sample No.	**Phase**											
K1	Metallic iron											
	Bright-lamellar	avg ($n=3$)	–	–	–	–	–	–	80	–	–	–
		std	–	–	–	–	–	–	4	–	–	–
	Light grey	avg ($n=16$)	0.11	0.11	–	–	–	–	66	0.40	–	–
		std	0.02	0.00	–	–	–	–	1	0.03	–	–
	Grey	avg ($n=9$)	0.08	0.08	0. 17	–	–	–	55.5	0.50	–	–
		std	0.01	0.00	0.03	–	–	–	0.4	0.05	–	–
K2	Metallic iron											
	Bright-lamellar	avg ($n=4$)	–	–	–	–	0.26	0.50	86	–	–	1.9
		std	–	–	–	–	0.04	0.05	3	–	–	0.1
	Light grey	avg ($n=9$)	–	–	–	–	0.20	–	65	–	–	–
		std	–	–	–	–	0.02	–	2	–	–	–
	Grey	avg ($n=7$)	–	0.16	0.12	–	0.4	–	56	–	–	1.5
		std	–	0.02	0.01	–	0.3	–	2	–	–	0.3
K3	Metallic iron	avg ($n=5$)	–	–	–	–	–	0.5	99.3	–	–	–
		std	–	–	–	–	–	0.1	0.1	–	–	–
	Bright-lamellar	avg ($n=9$)	–	–	–	–	–	0.5	93.2	–	–	–
		std	–	–	–	–	–	0.1	0.8	–	–	–
	Light grey											
	Grey	avg ($n=3$)	–	0.20	–	–	–	0.3	58	0.39	–	–
		std	–	0.08	–	–	–	0.1	1	0.03	–	–
K4	Metallic iron	avg ($n=24$)	–	–	–	–	–	–	99.1	0.73	–	–
		std	–	–	–	–	–	–	0.8	0.04	–	–
	Bright-lamellar	avg ($n=3$)	–	–	0.18	–	–	–	62	–	–	–
		std	–	–	0.04	–	–	–	1	–	–	–
	Light grey	avg ($n=8$)	–	–	0.3	–	–	–	65	–	–	–
		std	–	–	0.1	–	–	–	2	–	–	–
	Grey	avg ($n=34$)	0.2	0.12	0.3	0.15	–	–	58	0.6	0.46	–
		std	0.1	0.2	0.1	0.00	–	–	2	0.1	0.02	–
K5	Metallic iron	avg ($n=2$)	–	–	0.12	–	–	–	97.9	–	–	–
		std	–	–	0.00	–	–	–	0.7	–	–	–
	Bright-lamellar	$n=1$	–	–	–	–	–	–	79.5	–	–	–
	Light grey	avg ($n=28$)	0.10	0.14	0.2	–	–	–	68	0.5	–	-
		std	0.02	0.06	0.1	–	–	–	1	0.1	–	–
	Grey	avg ($n=22$)	0.08	0.16	0.3	–	–	–	55	0.44	–	–
		std	0.01	0.07	0.2	–	–	–	2	0.07	–	–

Table 2 (continued)

			Cl	K	Ca	Ti	Cr	Mn	Fe	Co	Ni	Cu
	wt.%Sigma (min–max)		0.03–0.09	0.04–0.10	0.04–0.10	0.05–0.12	0.05–0.13	0.1–0.2	0.3–1.0	0.17–0.38	0.1–0.3	0.3–1.0
K6	Metallic iron	avg ($n=3$)	–	–	–	–	–	–	96	–	–	–
		std	–	–	–	–	–	–	1	–	–	–
	Bright-lamellar	avg ($n=11$)	–	–	–	–	–	–	70	–	–	–
		std	–	–	–	–	–	–	2	–	–	–
	Light grey	avg ($n=16$)	–	–	0.16	–	–	–	65	1.5	–	–
		std	–	–	0.05	–	–	–	2	0.2	–	–
	Grey	avg ($n=19$)	0.11	0.10	0.17	–	–	–	56	1.2	–	–
		std	0.02	0.03	0.04	–	–	–	2	0.2	–	–

wt.%Sigma (min–max): The range of standard error which is acquired from the EDS software

–: not available for discussion since the element concentration remains below the wt.% sigma deviation

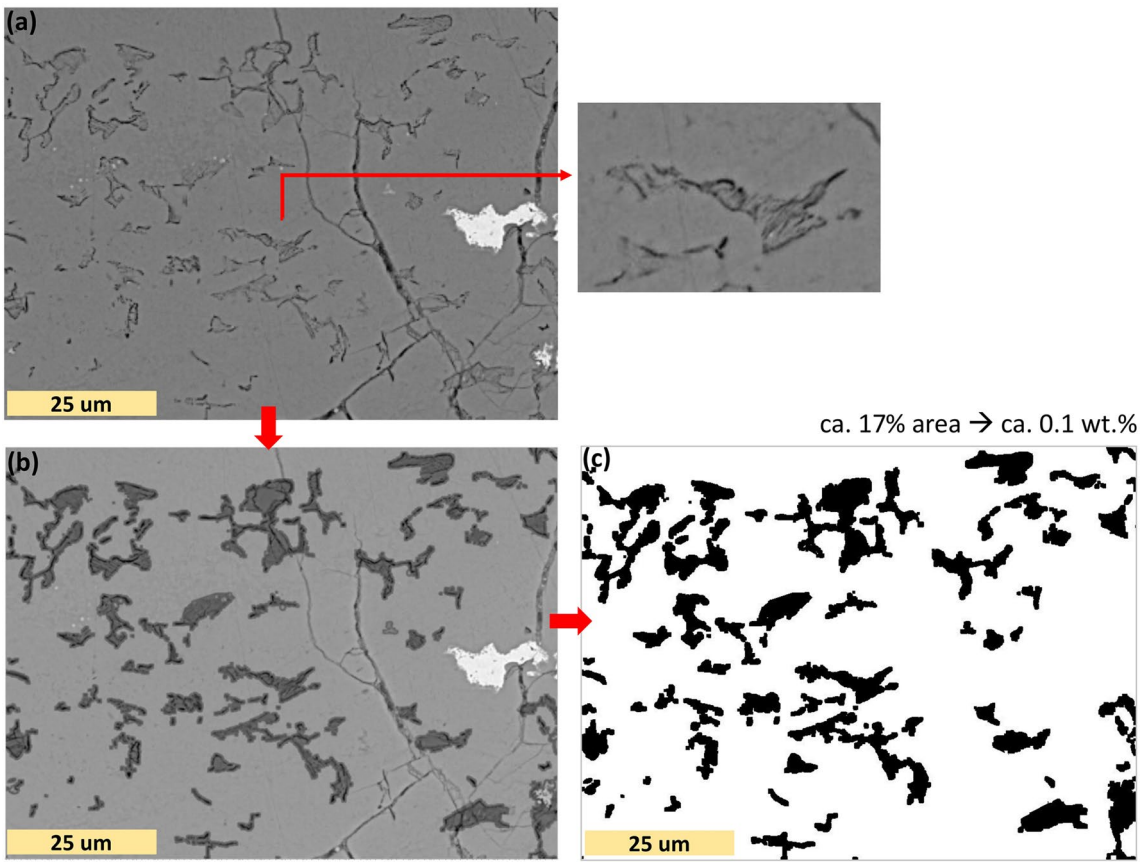

Fig. 3 (**a**) BSE image showing the pearlite remnants in lamellar pattern on the sample surface of the artefact K4, (**b**) Image showing the relatively distinguished pearlite remnants after the image analysis, in which cracks and small preserved iron were excluded, (**c**) the estimation of C content based on the relative percentage of pearlite remnants over the sample surface

content on the sample surface. At the end, the distribution of all these analysed areas was reviewed to determine how homogeneously scattered these areas were on the sample surface. The C content and distribution was thus estimated semi-quantitatively, considering the obstacles caused by the corrosion of the sample surface, the degeneracy of pearlite remnants, and the spheroidization of cementite.

Result and Discussion

Meteoric Source

Since iron meteorite is composed of Ni–Fe alloy [26], a high Ni concentration of around 6–20 wt.% is assumed to originate from a meteoric source [36]. However, Jambon [30] points out that Ni values could diminish during the weathering of a given iron artefact. The study reported a wide range of Ni concentrations for the iron objects from the Bronze Age, with high Ni concentrations in the uncorroded parts and low concentrations (even < 1 wt.%) in the corroded parts of a given iron artefact. The ratio of Fe:Ni:Co for the weathered iron artefacts from the Bronze Age were also found to have similar trends with weathered iron meteorites [30]. Together such evidence indicates that Ni abundance alone cannot be used to rule out a meteoritic origin for iron artefacts [30]. Instead, Co should also be examined, along with Fe and Ni, and Ni concentrations of different regions of the artefact should be assessed in context of the corrosion observed within these regions [30]. The Fe, Ni and Co concentrations of the EBA iron artefact K6 in Akanuma [25] are compared with meteoritic iron data from Jambon [30], and the results confirmed that the concentrations are consistent with terrestrial sources and not iron meteorites.

In the current study, EDS analysis was conducted on both the corroded parts and metallic iron islands if any were preserved in the artefacts. The results of 205 point-analyses indicate that the Ni (0–0.49 wt.%) and Co (0–1.79 wt.%) concentrations within the iron artefacts are very low, mostly being below the detection limit of the instrument.

Furthermore, Widmanstätten structure with Ni-rich kamacite and taenite bands was not detected for any of the artefacts. However, since the Widmanstätten structure might be demolished during the smithing process at a high temperature (e.g. around 1000 °C) [28], the presence of other mineral phases, which could be observed in meteoritic-sourced artefacts, was also considered in the current study. Such meteoritic phases include: cohenite $(Fe, Ni)_3C$, schreibersite $(Fe,Ni)_3P$, chalcopyrite ($CuFeS_2$) and troilite (FeS), which are observed in ancient iron artefacts made from meteorites [7, 28, 29, 37]. However, any composition related to these phases was not detected. Any weathered Ni-rich mineral phases like gamma-$(Fe,Ni)_2O_3$ [38, 39] were also not observed in the corroded parts of the artefacts. Therefore, it is unlikely that the early iron artefacts from Kaman-Kalehöyük were made from materials of a meteoric iron source.

Dominant Phases

After analysis of the iron objects by SEM–EDS, four main phases were determined: (1) metallic iron, (2) corrosion products (3) slag inclusions, and (4) cementite (Fig. 4).

Metallic Iron

Two iron artefacts K3 and K4 are mainly composed of the metallic iron preserved. In the MBA artefact K3, corrosion started to penetrate up to 25 µm from the edge. In the MBA artefact K4, a considerable amount of corrosion penetrated from the edge towards the centre of the artefact. Other artefacts were completely corroded, with only very tiny islands of ferrite (2.5–5 µm in size) being found within some of them (Fig. 5). As a result of their small size, carbon and oxygen contribution from the surrounding iron oxide matrix with cementite lamella might affect the EDS results (Table 2, Figs. 5, 6).

Corrosion Products

At least some corrosion was observed in all of the artefacts. The main purpose of determining the composition of the corroded matrix was to establish the nature of the compositional difference between the bright lamellar structures and the surrounding corroded iron matrix, and to identify the main phases within the corrosion products. A series of spot analyses ($n = 3$–50 for each artefact, depending on the size and heterogeneity of the texture of the artefact) were performed on the corroded parts. Two sub-phases were mainly recognized on the corroded parts of the artefacts under SEM–EDS observation, and these were represented by light grey and grey phases on a back-scattered electron (BSE) image. The Fe content of the artefacts enabled these two sub-phases to be distinguished. The Fe content is equal to or greater than around 33 at. % for the light grey phase; and lower than around 33 at.% for the grey phase (Fig. 5). Due to the inability of the instrument to reliably estimate the ferric-ferrous ratio, it is difficult to determine the iron oxide phases on the corrosion precisely. However, to compare with the compositions of these phases observed by using SEM–EDS, the ideal compositions of iron oxides, magnetite (Fe_3O_4), maghemite (γ-Fe_2O_3) and goethite (α-FeO(OH)), which are generally observed in the corrosion of the iron objects from the literature [40–44], are shown in Fig. 5. As such, on comparison with the literature values, the results of the EDS analyses were found to be scattered within a certain range rather than exactly corresponding with the ideal ratios.

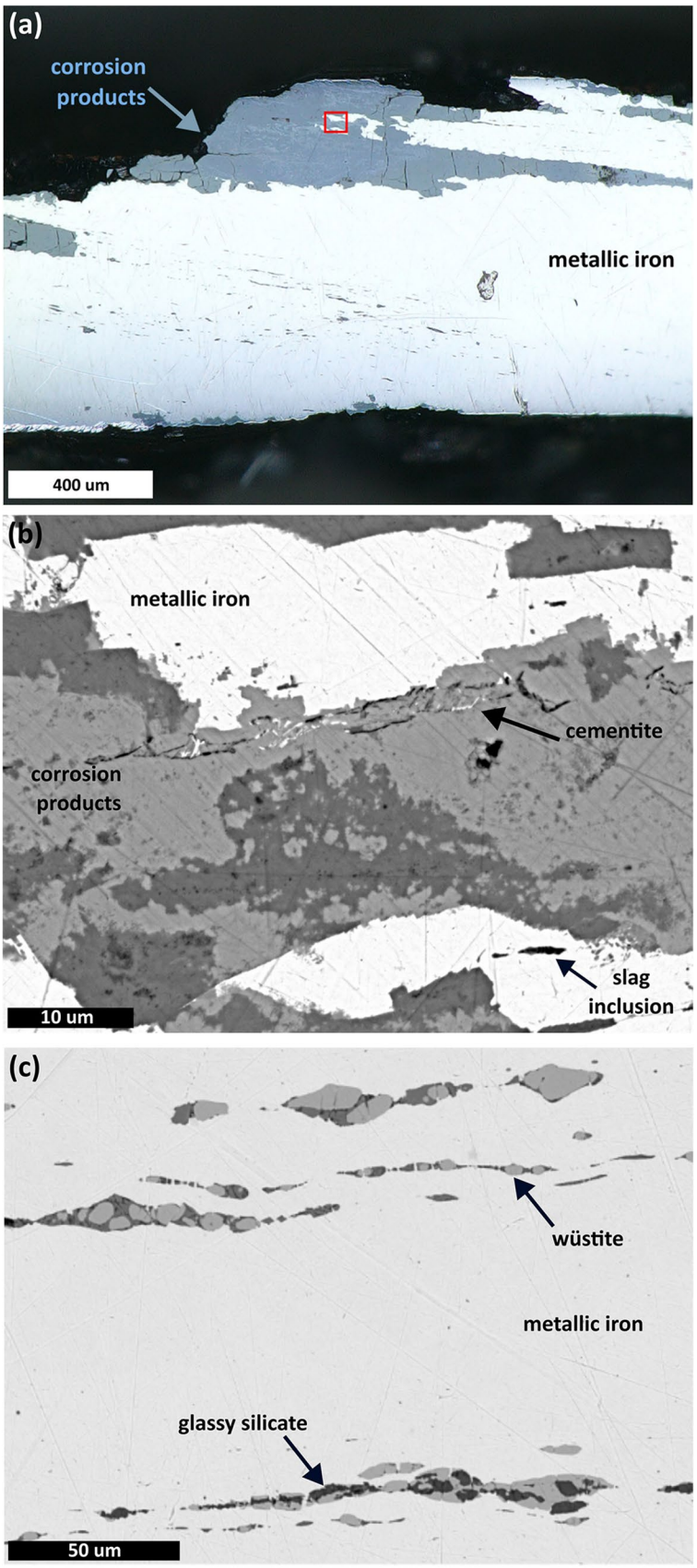

Fig. 4 (**a**) Optical microscope image of the artefact K4. The closer view of the rectangular area is shown in b. (**b**) The dominant phases in the iron artefacts on BSE image. Grey and light grey phases can be observed in the corrosion products. (**c**) Slag inclusions, composed of grey wüstite and dark grey silicate glass, in a parallel alignment

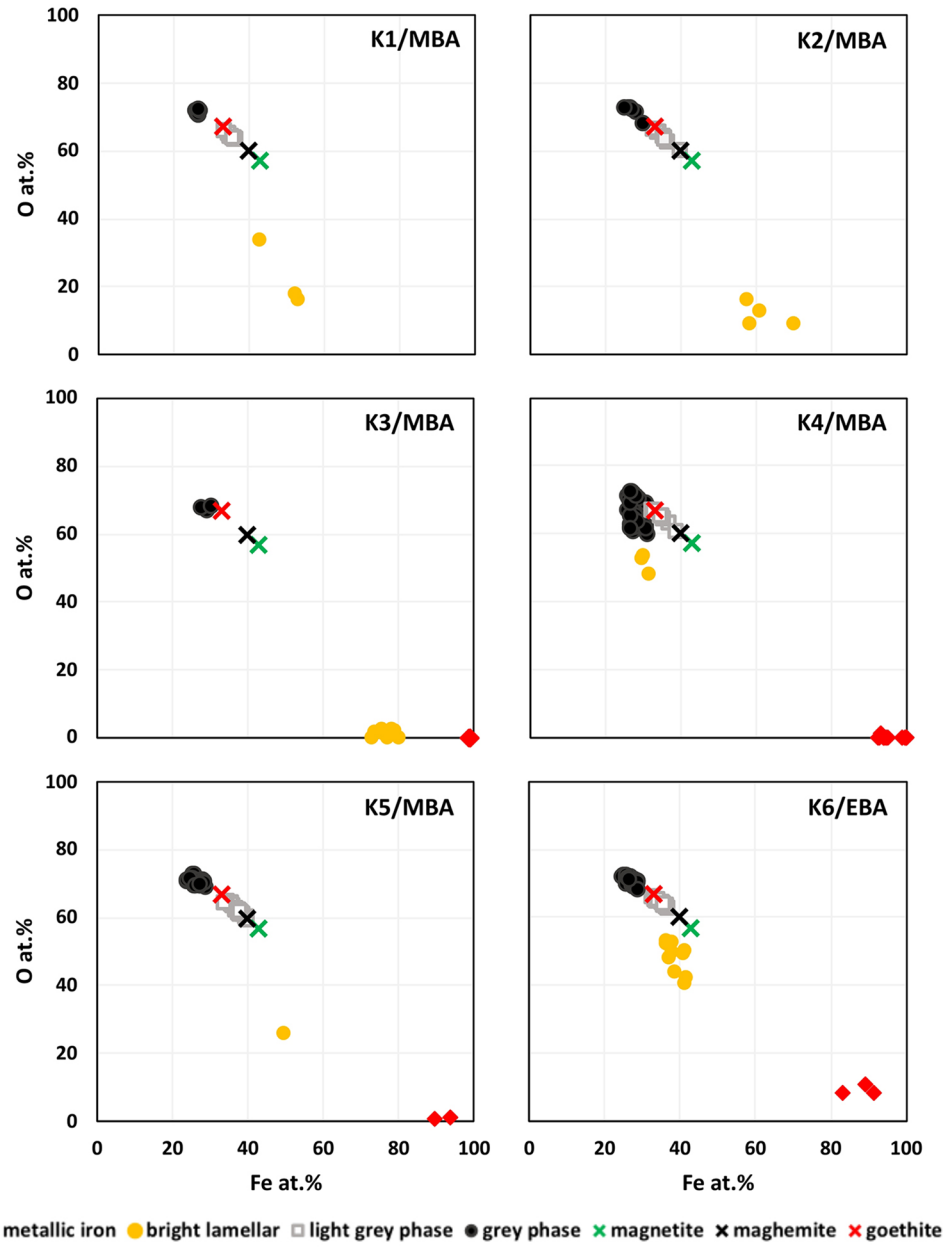

Fig. 5 Iron and oxygen contents (at.%) of the dominant phases in the iron artefacts

This is probably because the phases within the corrosion products are intermixed with each other at a smaller scale than the spatial resolution of our EDS analyses. Accordingly, Grevey et al. [44] applied X-ray diffraction, FE-SEM–EDS analysis and micro-Raman spectroscopy to examine such phases within the corrosion products, and found that the different iron oxide phases were intermixed, which would cause the EDS results spreading over the compositional ranges of the iron oxide phases. Such a finding also supports the occurrence of heterogeneously distributed iron oxide phases at the µm scale in our study. The lower Fe-content grey phase might contain a significant contribution of amorphous iron (oxy)hydroxides, when considering the long-term burial of the iron objects in soil and exposure to atmospheric conditions after their excavation and the results of previous studies. Indeed, such amorphous iron (oxy)hydroxide phases are observed in ancient iron materials exposed to soil and air [7, 43, 45, 46]. Therefore, a mixture of iron oxide and (oxy)hydroxide phases could be observed in the corroded portions of the artefacts.

Slag Inclusions

Slag inclusions were also recognized in all of the iron artefacts. The slag inclusions mostly exhibit nodular shape from less than 5 µm to a few ten µm in width. Only in the MBA artefact K4, the slag inclusions in the dendritic structure also occur, and demonstrate a parallel alignment

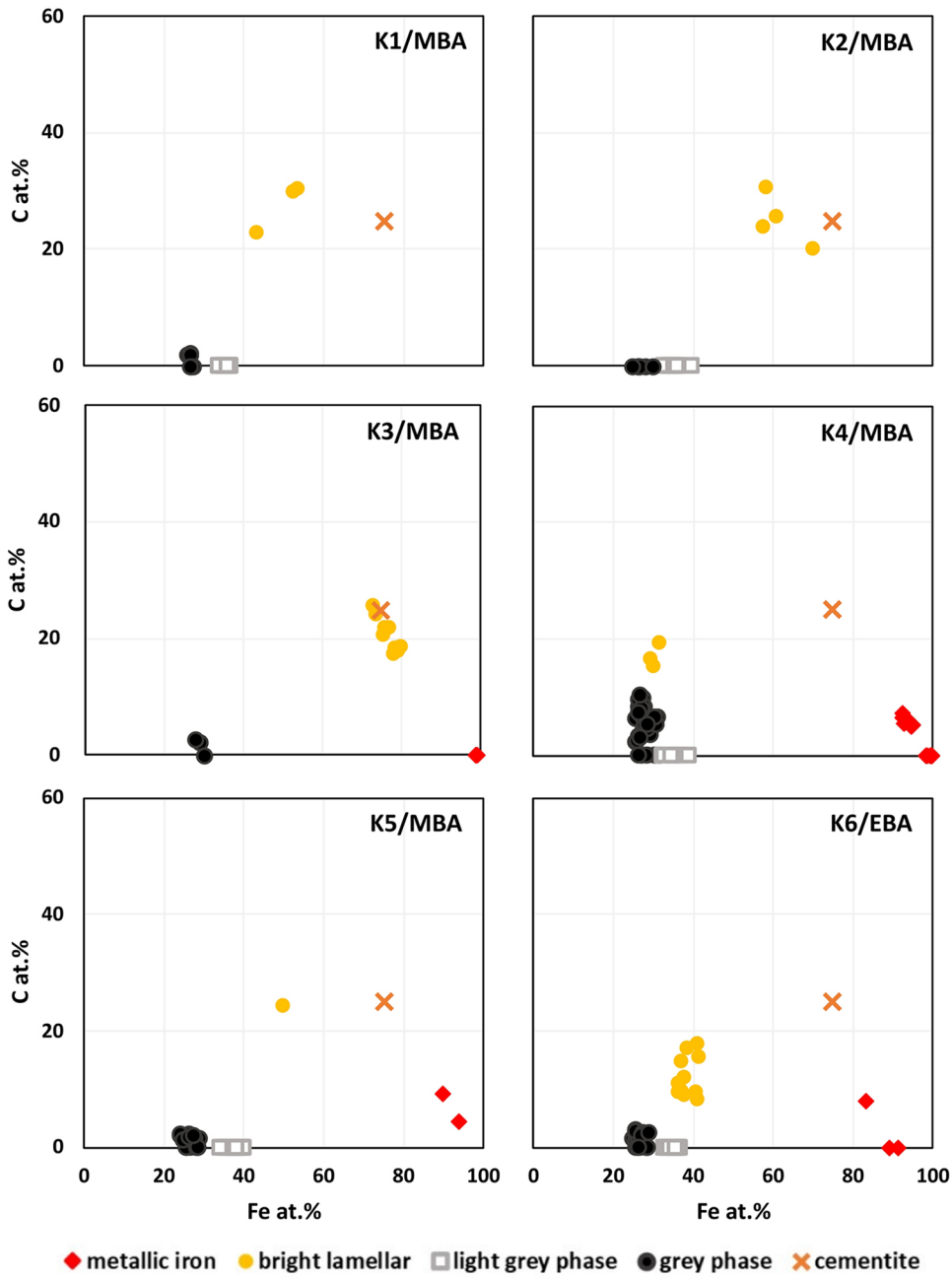

Fig. 6 Iron and carbon contents (at.%) of the dominant phases in the iron artefacts. Bright lamellar structures can be seen in Figs. 7 and 8

along the edge of the artefact (Fig. 4c). This artefact was the only sample which was cross-sectioned in a longitudinal direction. The slag stringers in a parallel alignment along the edges, which may have been generated by hammering, were thus clearly observed only in this artefact. Although the small sizes of the slag inclusions limited the precision of the EDS analysis, because of interferences from the surrounding iron oxide matrix [47], the slag inclusions were found to be composed mainly of wüstite (FeO) and silicate glass. The presence of trapped slag inclusions supports the idea that the early iron artefacts were produced by smelting [4, 36]. Nevertheless, such inclusions might also be formed while forge welding during the smithing process [4, 36]; hence, further analysis is necessary.

Cementite

The C-rich phase observed in bright lamellar structures (up to 1.5 µm in thickness) was recognized in all of the artefacts except the artefact K3 from the MBA, with cementite or pearlite remnants being a likely candidate for this phase. On

the artefact sample K3 mainly composed of metallic iron, the compositional difference between C-rich dark areas and bright areas with pure metallic iron was recognized by using SEM–EDS. However, it was difficult to trace their boundary precisely because of the limited polishing quality on a soft metallic surface, and chemical composition of the artefact was determined less precisely.

There are usually three main conditions in which cementite or pearlite structures can be observed in the corroded iron matrix [3, 4, 6]: (1) preserving the original composition, (2) being partially replaced by corrosion, and (3) being completely corroded, but still keeping the texture of the original structures. Therefore, the EDS spot analyses were performed on the bright lamellar structures corresponding to the first and second conditions. The results of EDS point-analyses (Fig. 6) indicated that the bright lamellar structures are richer in carbon than the surrounding iron oxide matrix, and contain a recognizable amount of oxygen (Fig. 5). Therefore, the bright lamellar components might have been oxidized throughout the burial period, but they still preserve their carbon content. Alternatively, the cementite or pearlite may be largely intact, but due to the small size of the features they are within, a contribution of the surrounding iron oxide matrix is also observed in the EDS spectrum (Figs. 6, 7).

Implications of the Presence of Cementite or Pearlite Remnants

The microtextures of the artefacts and the chemical compositions of the dominant phases suggest the presence of cementite or pearlite remnants in the iron artefacts. If this is the case, were the artefacts made of an iron alloy with carbon intentionally, at such early periods?

Scott [4] and Scott and Eggert [7] have pointed out that the random absorption of C into bloom occurs under a significantly C-enriched reducing environment inside the furnace, during *primary carburization*. Eliyahu-Behar et al. [48] have suggested that the C content of an iron artefact and its distribution within the sample matrix are required, in order to find out whether the steel composition was formed intentionally in the artefacts during the secondary smithing [2, 48] because the outer edge of the iron objects are usually intruded by corrosion. Additionally, any correlation between the artefact type and C content should also be checked to

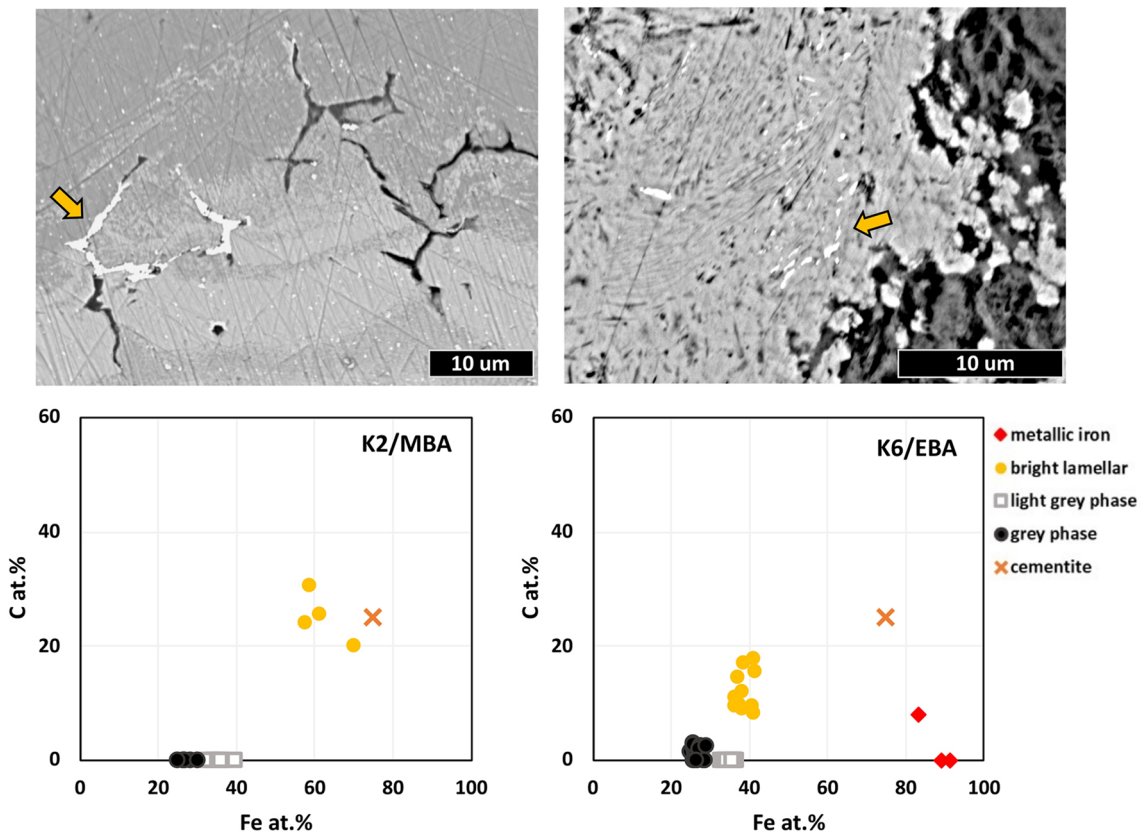

Fig. 7 The microtextures, and iron and carbon contents (at.%) of the dominant phases, including cementite remnants. Bright lamellar structures are pointed by the arrows on BSE images

further investigate whether *secondary carburization* was involved [48].

Considering the possible correlation between the artefact type and the C content for the assemblage of the iron artefacts in this study, the knife-shaped or pin-shaped artefacts are supposed to be harder and include a higher C content. On the other hand, the bar-shaped artefacts, as a semi-product, would not have a high C content for an easier smithing process, only if there was such an awareness among the metal workers at those periods.

The image analysis, which was undertaken to determine the C content of the samples and examine its distribution on the sample surfaces, indicated that the C content of the iron artefacts from the MBA ranged from less than 0.02 to 0.2 wt.%. The MBA knife-shaped artefact K1 contained a C content of between 0.06 and 0.2 wt.% (Fig. 8), and included regions with a low C steel composition, which resulted from the cementite and pearlite compounds having a heterogeneous distribution in the matrix.

The pin-shaped artefact K2, which was found from the same context as the knife-shaped artefact K1, consisted of only a few networks of cementite flakes (Fig. 8). These cementite flakes were distributed irregularly in the matrix. The C content estimated was less than 0.02 wt.%, which is comparable to the composition of ferrite. A similar composition within a few networks of cementite films could be observed in the iron materials with almost pure iron content in [49–51]. Therefore, this artefact was made from iron and does not contain any steel composition regions.

The artefacts K1 and K2 were the latest samples within the MBA group. On the other hand, the iron artefact K6 from the EBA demonstrates a high C content up to 0.6–0.8 wt.%, especially in the inner part of the artefact (Fig. 8). Akanuma [25] discovered that the artefact was a nicely formed prismatic bar, in terms of its shape, using X-ray photography. In the stratigraphy of the ancient mound, the iron artefact was uncovered from the Stratum IVa (Intermediate Period), in which the pottery assemblage consisted of both wheel-made pottery from the ACP and hand-made pottery from the EBA [31]. In the ancient texts from the ACP, a bar is one of the forms in which iron was traded [14]. Considering the probable morphology of the artefact and textual evidence, the iron artefact K6 could be an iron bar. However, if the intention was to produce an iron bar as a semi-product, it was supposed to have a low C content; hence, the intended final shape could be given later during secondary smithing. Such a high C content must have made the bar brittle and harder to give a shape later. From this perspective, its possible functional type does not match its high C content. When considering such early periods, the main aim would be to smelt the iron source. It must have still been hard to control the atmospheric conditions inside the furnace, which could be a bowl-furnace, a pit-furnace or a small shaft-furnace

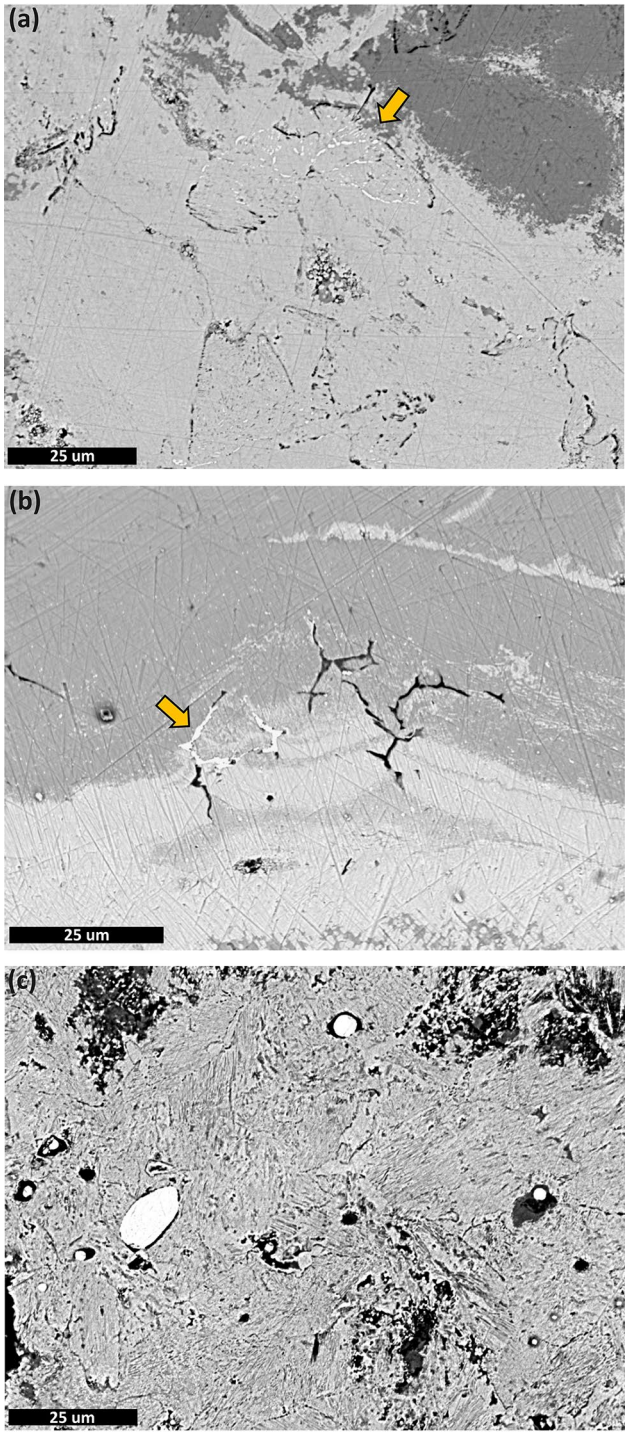

Fig. 8 Pearlite structures of the iron artefacts. (**a**) The knife-shaped artefact K1 from the MBA, (**b**) the pin-shaped artefact K2 from the MBA, (**c**) the bar-shaped artefact K6 from the EBA with bright and dark trapped slag inclusions. Bright lamellar structures are pointed by the arrows

[18, 52, 53]. As suggested in Scott [4], Scott and Eggert [7] and Eliyahu-Behar et al. [48], if it was a C-rich reducing atmosphere inside the furnace, the spontaneous absorption

of C from the furnace environment might have occurred in a small bloom that was subsequently forged into a bar-like shape. As also another archaeological evidence, Eliyahu-Behar et al. [54] pointed out the ancient blooms with C content up to 0.6–0.7 wt.% from the ancient sites Hazor and Beer-Sheba (Israel) to demonstrate that primary carburization could occur.

Considering the pin-shaped artefact K2 with a pure iron composition, the knife-shaped artefact K1 with low C content or the possibly bar-shaped artefact K6 with a high C content, it is still difficult to assert that they were produced as steel intentionally, because of the variety of C content among the artefacts and the lack of correlation between C content and artefact type. On the other hand, such a variation in C content, could simply be indicative of the large range in furnace conditions achieved by early smelters of iron artefacts. In the latter case, the varying conditions would have had major implications in terms of the C abundance acquired by a bloom during iron smelting in the Bronze Age. As a tentative suggestion here, the variation in C content might be one of the reasons behind the wide scale of prices for iron in the ancient texts, which was caused by the variation in purity or quality as discussed by Dercksen [14].

Conclusion

A group of iron artefacts, which were excavated from the MBA and EBA stratigraphic layers at Kaman-Kalehöyük in Central Anatolia, were re-analysed via a minimally invasive methodology in this study. The main aim was to describe the early iron artefacts in terms of their morphology, dominant mineral phases, C content and distribution, in order to discuss the state of iron production at such early periods, especially in terms of intentional carburization. After the SEM–EDS analysis, the composition and microstructure of the samples were determined, and it was concluded that the early iron artefacts are composed of iron and/or steel. Therefore, the ancient metal workers managed to smelt iron, but it is still difficult to tell if the early artefacts in this study were produced as steel intentionally, because of the variation in microstructures and C contents found within the artefacts. Such a finding could highlight the range in early efforts to smelt iron, while the ancient metal workers were trying to figure out how to control furnace conditions during the Bronze Age in Central Anatolia. Furthermore, the resulting variation in C content and the corresponding differences in the physical properties of such iron objects, suggests that varying iron quality could be responsible for the large disparity in the prices of iron artefacts recorded within ancient texts from the Bronze Age.

Acknowledgements We would also like to express our sincere thanks to the Japanese Institute of Anatolian Archaeology of the Middle Eastern Culture Centre in Japan, for the permission to undertake the analyses reported here on the samples and to the excavation team members for providing the archaeological and stratigraphic data of the artefacts. We would also like to extend our special thanks to Christian Potiszil for reviewing the manuscript and his valuable comments.

Funding Open access funding provided by Okayama University.

Open Access This article is licensed under a Creative Commons Attribution 4.0 International License, which permits use, sharing, adaptation, distribution and reproduction in any medium or format, as long as you give appropriate credit to the original author(s) and the source, provide a link to the Creative Commons licence, and indicate if changes were made. The images or other third party material in this article are included in the article's Creative Commons licence, unless indicated otherwise in a credit line to the material. If material is not included in the article's Creative Commons licence and your intended use is not permitted by statutory regulation or exceeds the permitted use, you will need to obtain permission directly from the copyright holder. To view a copy of this licence, visit http://creativecommons.org/licenses/by/4.0/.

References

1. R.F. Tylecote, Furnaces, crucibles and slags, in *The coming of the age of iron*. ed. by T.A. Wertime, J.D. Muhly (New Haven, London, 1980), pp.183–228
2. N. Yahalom-Mack, A. Eliyahu-Behar, The transition from bronze to iron in Canaan: chronology, technology, and context. Radiocarbon. **57**(2), 285–305 (2015)
3. R. Knox, Detection of iron carbide structure in the oxide remains of ancient steel. Archaeometry. (1963). https://doi.org/10.1111/j.1475-4754.1963.tb00578.x
4. B.G. Scott, The retrieval of technological information from corrosion products on early wrought iron artefacts, in *Evidence Preserved in Corrosion Products: New Field Studies in Artifact Studies, Proceedings of a Joint Conference Between UKIC Archaeology Section and the Council for British Archaeology Science Committee*. ed. R. Janaway, B. Scott (Leeds, 1983, 1989), pp. 8–14
5. R. Pleiner, *Iron in Archaeology: The European Bloomery Smelters* (Archeologický Ustav AVČR, Praha, 2000)
6. M.R. Notis, A Ghost Story: remnant structures in corroded ancient iron objects. MRS Online Proc. Lib. Arch. **712**, 259–267 (2002)
7. D.A. Scott, G. Eggert, *Iron and Steel: Corrosion, Colorants* (Conservation. Archetype Publications, London, 2009)
8. H. Genz, The Iron Age in central Anatolia, in *The Black Sea, Greece, Anatolia and Europe in the First Millennium BC*. ed. G.R. Tsetskhladze (Peeters, Leuven, Belgium; Paris, France; Walpole, MA, USA 2011), pp. 331–368
9. N. Erb-Satullo, The innovation and adoption of iron in the Ancient Near East. J. Archaeol. Res. **27**, 557–607 (2019)
10. J.D. Muhly, R. Maddin, T. Stech, E. Özgen, Iron in Anatolia and the nature of the Hittite iron industry. Anatol. Stud. **35**, 67–84 (1985)
11. J. Siegelova, H. Tsumoto, Metals and metallurgy in Hittite Anatolia, in *Insights into Hittite History and Archaeology*. ed. by H. Genz, D.P. Mielke (Peeters, Leuven-Paris-Walpole, MA, 2011), pp.275–300
12. R. Maxwell-Hyslop, The metals amūtum and aši'um in the Kültepe texts. Anatol. Stud. **22**, 159–172 (1972)
13. S. Çeçen, Kanis Karum'unun diğer karum ve wabartumlar'a "KUAN" (amutum) ile ilgili önemli talimatları (The instructions

about "KUAN" (amūtum) from Kanis-Karum to other karum and wabartum). Belleten. **231**(5), 219–232 (1997). (**in Turkish**)
14. J.G. Dercksen, Metals according to documents from Kültepe-Kanish dating to the Old Assyrian Colony Period, in *Anatolian Metal III*. ed. by Ü. Yalçın (Deutsches Bergbau Museum, Bochum, 2005), pp.17–34
15. K.R. Veenhof, A difficult Old Assyrian business venture, Mannum-kī-Aššur tries his luck with iron. Bibl. Orient. **73**(1–2), 14–40 (2016)
16. M.T. Larsen, *The archive of the Šalim-Aššur Family* (Türk Tarih Kurumu Basımevi, Ankara, 2010)
17. H. Erol, Old assyrian metal trade, its volume and interactions. Belleten. **298**(LXXXIII), 779–807 (2019)
18. D. Killick, From Ores to Metals, in *Archaeometallurgy in Global Perspective, Methods and Syntheses*. ed. by B.W. Roberts, C. Thornton (Springer-Verlag, New York, 2014), pp.11–46
19. H. Akanuma, Iron objects from the architectural remains of stratum III and stratum II at Kaman-Kalehöyük: correlation between composition and archaeological levels. Anatol. Archaeol. Stud. **11**, 191–200 (2002)
20. H. Akanuma, Further Archaeometallurgical study of 2nd and 1st millennium BC iron objects from Kaman-Kalehöyük, Turkey. Anatol Archaeol. Stud. **12**, 137–150 (2003)
21. H. Akanuma, Archaeometallurgical analysis of iron and copper objects from the stratum IIIb to stratum IIa at Kaman-Kalehöyük in 2001: correlation between composition and archaeological levels. Anatol. Archaeol. Stud. **13**, 163–174 (2004)
22. H. Akanuma, The Significance of the composition of excavated iron fragments taken from stratum III at the site of Kaman-Kalehöyük, Turkey. Anatol. Archaeol. Stud. **14**, 147–158 (2005)
23. H. Akanuma, Changes in iron use during the 2nd and 1st Millennia B.C. at Kaman-Kalehöyük, Turkey: composition of iron artifacts from Stratum III and Stratum II. Anatol. Archaeol. Stud. **15**, 207–222 (2006)
24. H. Akanuma, Analysis of iron and copper production activity in the central Anatolia during the Assyrian Colony Period. Anatol. Archaeol. Stud. **16**, 125–140 (2007)
25. H. Akanuma, The significance of Early Bronze Age iron objects from Kaman-Kalehöyük, Turkey. Anatol. Archaeol. Stud. **17**, 313–320 (2008)
26. G. Rapp, *Archaeomineralogy*, 2nd edn (Springer-Verlag, Berlin, Heidelberg, 2009)
27. J.K. Bjorkman, Meteors and meteorites in the ancient Near East. Meteoritics. **8**, 91–132 (1973)
28. E. Photos, The question of meteoritic versus smelted nickel-rich iron: archaeological evidence and experimental results. World Archaeol. **20**, 403–421 (1989)
29. T. Rehren, T. Belgya, A. Jambon, G. Káli, Z. Kasztovszky, Z. Kis, I. Kovács, B. Maróti, M. Martinón-Torres, G. Miniaci, V.C. Pigott, M. Radivojević, L. Rosta, L. Szentmiklósi, Z. Szőkefalvi-Nagy, 5,000 years old Egyptian iron beads made from hammered meteoritic iron. J. Archaeol. Sci. **40**, 4785–4792 (2013)
30. A. Jambon, Bronze Age iron: meteoritic or not? a chemical strategy. J. Archaeol. Sci. **88**, 47–53 (2017)
31. S. Omura, Kaman-Kalehöyük excavations in central Anatolia, in *The Oxford Handbook of Ancient Anatolia (10,000–323 BCE)*. ed. by S.R. Steadman, J.G. McMahon (Oxford University Press, Oxford, 2011), pp.1095–1111
32. S. Atsumi, M. Yoneda, Y. Shibata, I. Nakai, 中央アナトリア,カマン•カレホユック遺跡における青銅器時代の放射性炭素年代による編年 (Radiocarbon chronology on Bronze Age at Kaman-Kalehöyük in the central Anatolia). 考古学と自然科学 Archaeol. Nat. Sci. **57**, 37–53 (2008). (**in Japanese with the abstract in English**)
33. S. Omura, 2007 Yılı Kaman-Kalehöyük Kazıları (2007 Kaman-Kalehöyük Excavation Report). Kazı Sonuçları Toplantısı. **30**(3), 197–205 (2009). (**in Turkish**)
34. S. Omura, 2010 Yılı Kaman-Kalehöyük Kazıları (2010 Kaman-Kalehöyük Excavation Report). Kazı Sonuçları Toplantısı. **30**(3), 447–462 (2011). (**in Turkish**)
35. D.A. Scott, *Metallography and Microstructure of Ancient And Historic Metals* (Getty Publications, Singapore, 1991)
36. Ü. Yalçin, Early iron metallurgy in Anatolia. Anatol. Stud. **49**, 177–187 (1999)
37. K. Chen, Y. Wanga, Y. Liub, J. Mei, T. Jiang, Meteoritic origin and manufacturing process of iron blades in two Bronze Age bimetallic objects from China. J. Cult. Herit. **30**, 45–50 (2018)
38. D. Tilley, A. Bevan, The prolonged weathering of iron and stony-iron meteorite and their nomalous contribution to the Australian regolith, in *New approaches to an old continent Proceedings of the 3rd Australian Regolith Conference Kalgoorlie Canberra*. ed. by G.Taylor, C.F. Pain (Cooperative Research Centre for Landscape Evolution & Mineral Exploration (CRC LEME), Perth WA, 1998), pp. 77–88
39. D. Johnson, J. Tylsesley, T. Lowe, P.J. Withers, M.M. Grady, Analysis of a prehistoric Egyptian iron bead with implications for the use and perception of meteorite iron in ancient Egypt. Meteorit. Planet. Sci. **48**, 997–1006 (2013)
40. D. Neff, S. Reguer, L. Bellot-Gurlet, P. Dillmann, R. Bertholon, Structural characterisation of corrosion products on archaeological iron. An integrated analytical approach to establish corrosion forms. J. Raman Spectrosc. **35**(8–9), 739–745 (2004)
41. D. Neff, P. Dillmann, L. Bellot-Gurlet, G. Beranger, Corrosion of iron archaeological artefacts in soil: characterisation of the corrosion system. Corros. Sci. **47**, 515–535 (2005)
42. L. Bellot-Gurlet, D. Neff, S. Réguer, J. Monnier, M. Saheb, P. Dillmann, Raman studies of corrosion layers formed on archaeological irons in various media. J. Nano RES-SW. **8**, 147–156 (2009)
43. J. Monnier, D. Neff, S. Réguer, P. Dillmann, L. Bellot-Gurlet, E. Leroy, E. Foy, L. Legrand, I. Guillot, A corrosion study of the ferrous medieval reinforcement of the Amiens cathedral. Phase characterisation and localization by various microprobes techniques. Corros. Sci. **52**(3), 695–710 (2010)
44. A.L. Grevey, V. Vignal, H. Krawiec, P. Ozga, K. Peche-Quilichini, A. Rivalan, F. Mazière, Microstructure and long-term corrosion of archaeological iron alloy artefacts. Herit. Sci. (2020). https://doi.org/10.1186/s40494-020-00398-9
45. J.M. Cronyn, *The Elements of Archaeological Conservation* (Routledge, London, New York, 1990)
46. M. Boucher, P. Dillmann, D. Delphine Neff, New insights in the long-term atmospheric corrosion mechanisms of low alloy steel reinforcements of cultural heritage buildings. Materials. (2017). https://doi.org/10.3390/ma10060670
47. I. Stepanov, L. Weeks, K. Franke, C. Cable, B. Overlaet, P. Magee, M. Händel, Y. Al Aali, M. Radwan, H. Zein, Methodologies for the investigation of corroded iron objects: examples from prehistoric sites in South-eastern Arabia and Western Iran. Sci. Technol. Archaeol. Res. **3**(2), 270–284 (2018)
48. A. Eliyahu-Behar, N. Yahalom-Mack, Revaluating early iron-working skills in the Southern Levant through microstructure analysis. J. Archaeol. Sci. Rep. **18**, 447–462 (2018)
49. B.G. Scott, *Early Irish Ironworking* (Ulster Museum, Belfast, 1990)
50. L.E. Samuels, *Light Microscopy of Carbon Steels* (ASM International, USA, 1999)
51. G.F. Vander Voort, *Metallography and Microstructures, ASM Handbook*, vol 9 (ASM International, USA, 2004)

52. B. Girbal, Experimenting with the bowl furnace, in *Accidental and Experimental Archaeometallurgy*. ed. by R.C.P. Doonan, D. Dungworth (HMS Occasional Publications, London, 2013), pp.83–92
53. D. Dungworth, Who's afraid of the bowl furnace? Hist. Metall. **48**, 1–7 (2015)
54. A. Eliyahu-Behar, N. Yahalom-Mack, Y. Gadot, I. Finkelstein, Iron smelting and smithing in major urban centers in Israel during the Iron Age. J. Archaeol. Sci. **40**, 4319–4330 (2013)

Publisher's Note Springer Nature remains neutral with regard to jurisdictional claims in published maps and institutional affiliations.